

pubs.acs.org/JACS Article

Duplex DNA Is Weakened in Nanoconfinement

Sagun Jonchhe, Shankar Pandey, Deepak Karna, Pravin Pokhrel, Yunxi Cui, Shubham Mishra, Hiroshi Sugiyama,* Masayuki Endo,* and Hanbin Mao*



Cite This: https://dx.doi.org/10.1021/jacs.0c01978



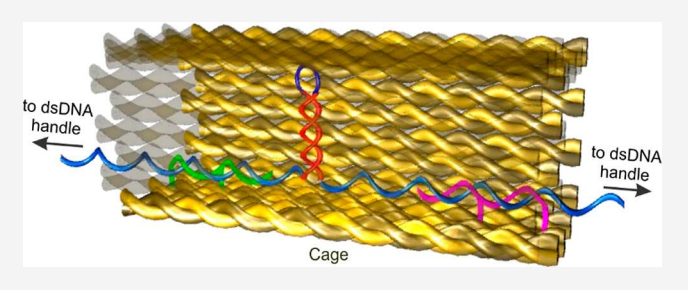
ACCESS

III Metrics & More

Article Recommendations

Supporting Information

ABSTRACT: For proteins and DNA secondary structures such as G-quadruplexes and i-motifs, nanoconfinement can facilitate their folding and increase structural stabilities. However, the properties of the physiologically prevalent B-DNA duplex have not been elucidated inside the nanocavity. Using a 17-bp DNA duplex in the form of a hairpin stem, here, we probed folding and unfolding transitions of the hairpin DNA duplex inside a DNA origami nanocavity. Compared to the free solution, the DNA hairpin inside the nanocage with a 15 \times 15 nm cross section showed a drastic decrease in mechanical $(20 \rightarrow 9 \text{ pN})$ and thermodynamic $(25 \rightarrow 6 \text{ pN})$



kcal/mol) stabilities. Free energy profiles revealed that the activation energy of unzipping the hairpin DNA duplex decreased dramatically ($28 \rightarrow 8 \text{ kcal/mol}$), whereas the transition state moved closer to the unfolded state inside the nanocage. All of these indicate that nanoconfinement weakens the stability of the hairpin DNA duplex to an unexpected extent. In a DNA hairpin made of a stem that contains complementary telomeric G-quadruplex (GQ) and i-motif (iM) forming sequences, formation of the Hoogsteen base pairs underlining the GQ or iM is preferred over the Watson–Crick base pairs in the DNA hairpin. These results shed light on the behavior of DNA in nanochannels, nanopores, or nanopockets of various natural or synthetic machineries. It also elucidates an alternative pathway to populate noncanonical DNA over B-DNA in the cellular environment where the nanocavity is abundant.

■ INTRODUCTION

Elucidating the property of duplex DNA in nanoconfinement is of fundamental importance in many fields ranging from singlemolecule biophysics to DNA sequencing. Recently, individual DNA molecules have been stretched inside nanochannels to investigate the interaction between proteins and DNA. Biochemical reactions such as enzymatic digestions and RNA transcriptions can also be investigated using confined DNA templates. In approaches leveraged for next-generation sequencing, DNA strands are guided through nanopores or nanochannels for accurate reading of individual bases or specific DNA segments.^{2,3} Results from these experiments are often interpreted with the speculation that the behavior of DNA inside the nanoconfinement remains the same as that in free solutions. Changes in the stability of duplex DNA bring complexity to these processes. Inside cells, DNA strands are often constricted in nanocavities of DNA binding proteins or DNA processing machineries. In telomerase for example, a semienclosed pocket exists to clasp the telomere DNA template.⁴ In polymerases, nanometer-sized reaction sites are abundant for DNA strands. Therefore, it is necessary to reveal the behavior of confined B-DNA duplex to fully understand these fundamental biochemical processes.

Nanoconfinement is known to increase the stability of proteins⁵⁻⁷ and non-B DNA structures such as G-quadruplexes and i-motifs.⁸⁻¹¹ These species share one common feature: water molecules are lost during the folding.^{12,13} Inside the

nanocavity with hydrophilic walls such as those found in DNA origami nanoassemblies, water molecules become increasingly ordered when the cavity gets smaller due to increased iondipole interactions. The resultant decreased water activity in the smaller cavity provides a driving force to accommodate released water molecules during folding of macromolecules, which increase the stabilities of the macromolecules. In duplex DNA, although there is a net release of water molecules during DNA hybridization, ¹⁴ the interaction of water molecules to the minor groove of dsDNA gets stronger, whereas no significant change is observed elsewhere in the structure. 15 Reduced water activity may also compromise the duplex DNA stability by weakening its base stacking. 16 In addition, various reports on the stabilization or destabilization of duplex DNA in solutions of negatively charged nanoparticles or polymers suggest complex cosolute effects on DNA properties. ¹⁷⁻¹⁹ It is therefore difficult to predict the effect of the nanoconfinement on the property of the DNA duplex.

In this work, we quantify for the first time the stability of B-DNA in the stem of the DNA hairpin in the nanocavity. The

Received: February 19, 2020 Published: May 8, 2020



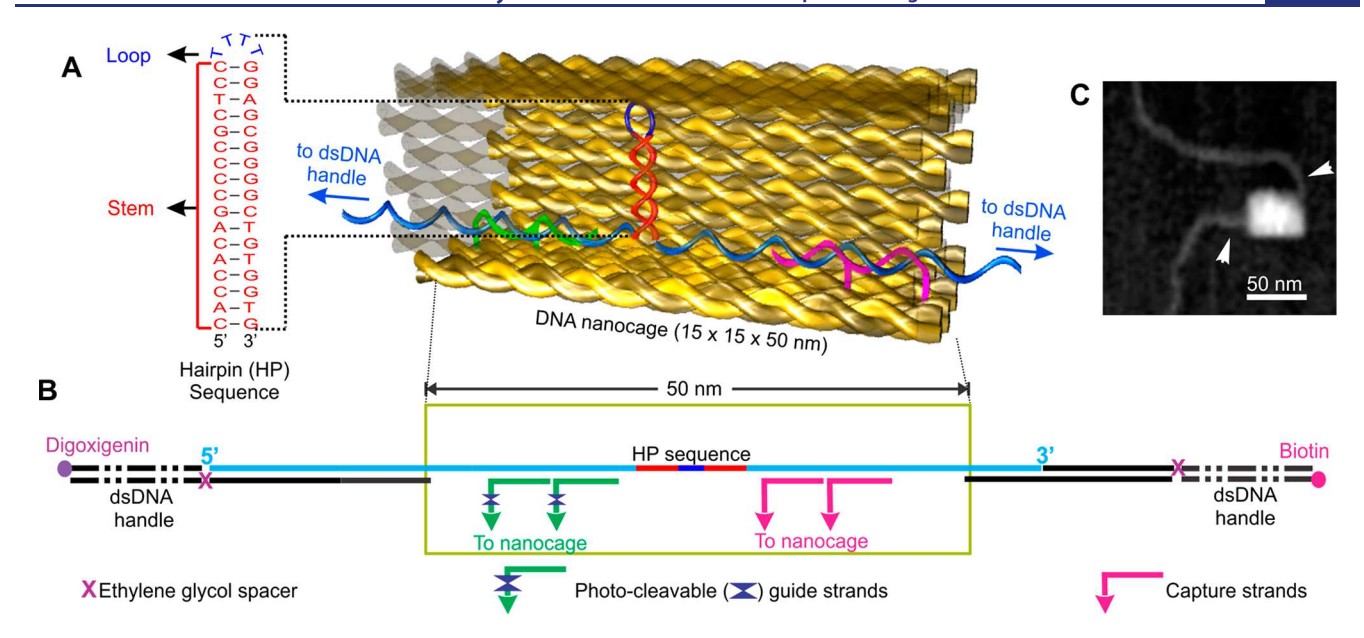


Figure 1. Design and characterization of the hairpin@nanocage construct. (A) Schematic of the DNA construct containing a hairpin-forming sequence inside the DNA nanocage. Sequence of the DNA hairpin is shown to the left. (B) Hairpin-forming sequence (taken from the bcl-2 promoter) inside the nanocage with two dsDNA handles, which are labeled with biotin and digoxigenin at the two ends, respectively, for affinity attachments. (C) AFM image of a nanocage after annealing with dsDNA handles (arrowheads).

DNA hairpin is made of a duplex DNA stem with a singlestranded loop. Upon unfolding of the hairpin, the Watson-Crick base pairs in the stem dehybridize whereas the loop remains single stranded. Therefore, the stability of the hairpin is governed by the stem. Since the hairpin stem is stabilized by the same Watson-Crick base pairs and base stacking in double-stranded B-DNA, 16 it has been well accepted that the DNA hairpin stem is a good mimic of the B form of DNA.²⁰ Here, we placed a DNA hairpin inside a DNA origami nanocage with a 15 × 15 nm cross section. Using mechanical unfolding in an optical tweezers instrument, we found that the mechanical stability of the hairpin decreases from 20.2 pN outside the nanocage to 9.4 pN inside the nanocage, which demonstrated that duplex DNA became weakened to an unexpected level in nanoconfinement. Using population analyses, we retrieved unfolding free energy trajectories of free and confined DNA hairpins. We found that the energy barrier to unfold DNA hairpins is much reduced in nanocages compared to free solutions. Next, we compared the formation of the B-DNA with non-B DNA using a hairpin that contains G-quadruplex and i-motif forming sequences in the two complementary stem strands. We revealed that inside the nanocage only 2% population was hairpin duplex, whereas 62% was tetraplex structures. These findings shed light on the property of physiologically prevalent B-DNA inside nanochannels, nanopores, or nanopockets of natural or synthetic machineries. Given the abundance of DNA sequences with a propensity to form noncanonical DNA structures in human genome, 21 our finding reveals a new physiological situation in which non-B DNA structures are preferred over the B form of

MATERIALS AND METHODS

Materials. All of the chemicals, unless specified, were purchased either from VWR or Nacalai Tesque. Bovine serum albumin (BSA, biotechnology grade) was purchased from Amresco. p8064 plasmid and all DNA staples were purchased from Eurofins Genomics. All of the oligos modified with biotin, digoxigenin, photocleavable linker,

and PEG linker were obtained from Japan Bio Services. The pET-26b (+) plasmid for handle preparation was obtained from Novagen. The Sephacryl S-300 and the gel-filtration column were purchased from GE Healthcare and Bio-Rad Laboratories, respectively. The streptavidin- or antidigoxigenin-coated polystyrene beads were purchased from Spherotech.

Synthesis of the DNA Origami Nanocages That Contain the Hairpin Hosting DNA Fragment. The DNA nanocage structures were designed using the protocol described elsewhere. In short, for the preparation of each nanocage (Figure 1), p8064 plasmid was digested with specific restriction enzymes in the presence of complementary primer strands shown in Table S1. The scaffold ssDNA was purified by agarose gel followed by quantification. For the synthesis of nanocage, 25 nM DNA scaffold was isothermally assembled at 50 °C for 1 h with 0.2 µM staple sequences (see Table S2) to form open nanocages. The hairpin forming sequences (see Figure S3, the stem region was taken from the sequence of the bcl-2 promotor;²² and Figure S4, the stem contained human telomeric tetraplexes sequences) were placed inside the open nanocage with the help of two photocleavable guides and two capture strands (Figures S1 ad S2) followed by closing of the nanocage using 4 equiv of closing staples (see Tables S2). The product was purified by a hand-packed Sephacryl S-400 gel-filtration column. The purified nanocages were annealed with two double-stranded DNA handles (each 2520-bp in length) by slowly cooling the mixture from 40 to 15 $^{\circ}$ C at a rate of -1

Characterization of the Single-Molecule DNA Nanocage Constructs by AFM. AFM images (Figures 1c and S5) were obtained at a scan rate of 0.2 frames per second (fps) in an AFM system (Nano Live Vision, RIBM, Tsukuba, Japan) with a silicon nitride cantilever (resonant frequency = 1.0–2.0 MHz, spring constant = 0.1–0.3 N/m, EBD tip radius < 15 nm, Olympus BLAC10EGS-A2). Sample preparation for imaging was done by adsorption of 2 μ L of sample onto a freshly cleaved mica plate [Φ 1.5 mm, pretreated with 0.1% 3-aminopropyl trimethoxysilane (APTES)] for 5 min at room temperature followed by several washings with 20 mM Tris buffer (pH 7.8) containing 10 mM MgCl₂ and 1 mM EDTA.

Mechanical Unfolding Experiments in Optical Tweezers. First, 0.5 μ L of sample was exposed to 365 nm UV for 10 min to break the photocleavable linker X in guide strands to avoid unwanted strain on the nanocage during mechanical unfoldings. By incubation

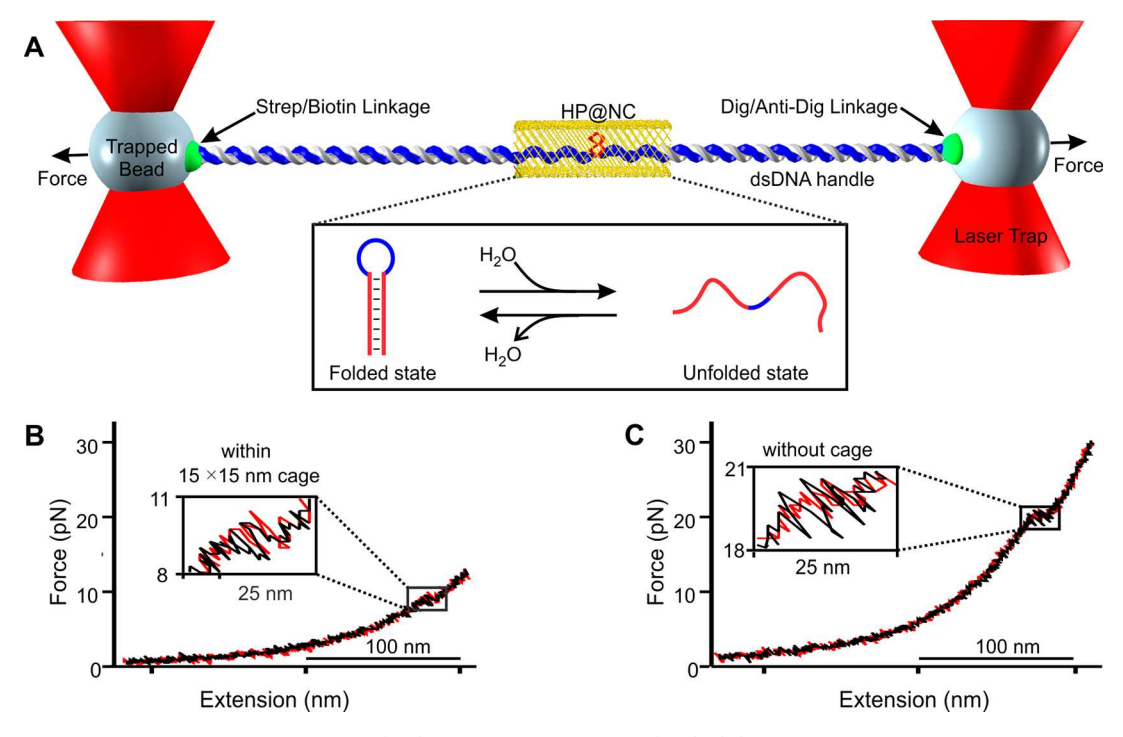


Figure 2. Mechanical unfolding of the bcl-2 hairpin (HP) within DNA nanocage (NC). (A) DNA construct in Figure 1 is tethered between two optically trapped beads via affinity interactions. (Inset) Unfolding and refolding transitions of the hairpin inside the nanocage (HP@NC). Strep, Dig, and Anti-Dig represent streptavidin, digoxigenin, and antidigoxigenin, respectively. Force versus extension curve of the DNA hairpin (B) within and (C) without a 15 × 15 nm nanocage. Red and black traces indicate stretching and relaxing curves, respectively. Zigzag features in the insets depict rapid unfolding/refolding transitions. Experiments were performed in a 20 mM Tris buffer (pH 7.8) supplemented with 100 mM KCl, 10 mM MgCl₂, and 1 mM EDTA at 25 °C.

of the exposed sample with streptavidin-coated polystyrene bead, the construct was immobilized on the surface of the bead via streptavidin/ biotin linkage. The immobilized DNA on streptavidin-coated beads and the antidigoxigenin-coated beads without DNA were flowed into the top and bottom channels of the three-channel microfluidic chamber, respectively. These beads were flowed to the middle channel via two micropipettes (i.d. 25 μ m, King Precision Glass, Claremont, CA) connecting the top and bottom channels, respectively, to the middle channel. Each bead was separately trapped by a 1064 nm laser beam in a custom-made dual-trap laser tweezers. Two beads were brought closer to each other by a steerable mirror in the laser tweezers instrument to form a DNA tether by digoxigenin/antidigoxigenin interaction between the the free end of the DNA and the antidigoxigenin-coated bead. The tether was stretched and relaxed at a loading rate of \sim 5.5 pN/s by the same steerable mirror. The force versus extension (F-X) traces were recorded at 1000 Hz using a Labview program. The experiments were carried out in a 20 mM Tris (pH 7.8) buffer or a 10 mM MES (pH 5.5) buffer supplemented with 10 mM MgCl₂, 100 mM KCl, and 1 mM EDTA at 25 °C.

RESULTS

Preparation of DNA Hairpins Inside the DNA Origami Nanocage. Mechanical unfolding and refolding experiments were performed in an optical tweezers instrument described previously.²³ First, we placed a DNA hairpin sequence (5'-CACCACAGCCCCGCTCC-TTTT-GGAGCGGGGC-TGTGGTG, the stem sequence (underlined) is taken from the bcl-2 promoter) inside a DNA origami nanocage assembly^{8,9} (Figure 1a and 1b). Two ends of the hairpin stem were tethered to two duplex DNA handles, which were attached to the two optically trapped polystyrene beads by affinity linkages. Two sides of the nanocage were left open to allow the passage of each DNA handle. This design ensured that force is applied directly on the DNA hairpin for mechanical unfolding and

refolding experiments. To ensure that the DNA hairpin is contained inside the nanocage, the nanocage is always anchored to one of the DNA pulling handles via two capture strands close to the hairpin (see Figure 1b and SI for details). Molecular simulation revealed that the DNA hairpin formed inside a 9×9 nm nanocage (which is smaller than the 15×15 nm nanocage used here) is not sterically hindered (Figure S15). AFM images have revealed successful preparation of the origami construct (Figure 1c).

Mechanical Unfolding and Refolding of DNA Hairpins Inside the Nanocage. To start mechanical unfolding and refolding of individual DNA hairpins tethered between two optically trapped polystyrene particles (Figure 2a), we moved one of the trapped beads away from another using a steerable mirror at a load force of 5.5 pN/s. This increased the tension in the DNA construct until the hairpin was unfolded (Figure 2b and S10b, inset). As a control, the same experiments were carried out on the DNA construct without the nanocage (Figure 2c and S10a). Compared to the unfolding force of the hairpin without the nanocage (Figures 2 and 3b, 20.2 pN), it came to our attention that the unfolding force was significantly smaller for the hairpin inside the nanocage (9.4 pN). The same trend was observed for the refolding forces (18.5 vs 7.4 pN (without vs within nanocage) see Figure S6).

To explain the different transition forces between these two DNA samples, we analyzed structures formed within and without nanocage. Outside the nanocage, rapid and reversible folding and unfolding transitions were observed at 20.2 pN (Figures 2c and 3b), which were consistent with those observed for DNA hairpins.²⁰ When we plotted the change in contour length (ΔL) histogram, we found that ΔL (13.5–14.2

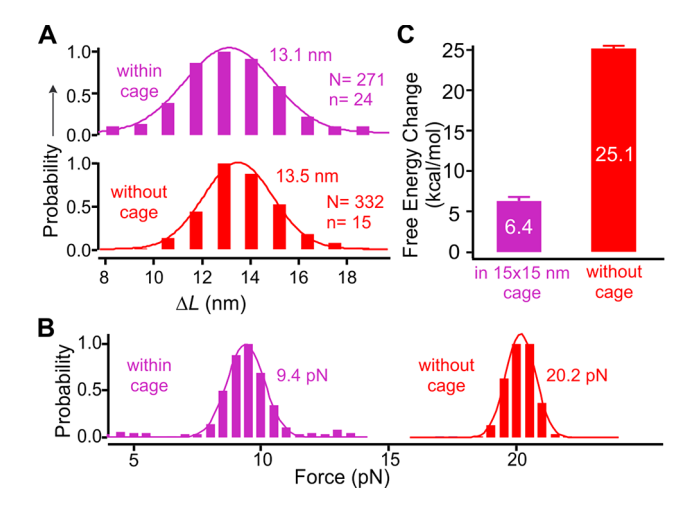


Figure 3. Mechanical properties of the bcl-2 hairpin within (purple) and without (red) the 15×15 nm nanocage. (A) Change in contour length (Δ L) and (B) unfolding force histograms of the bcl-2 hairpin inside and outside the nanocage. (C) Change in the free energy of unzipping the bcl-2 hairpin within (purple) and without (red) the nanocage. Solid curves depict Gaussian fittings. N and n depict the numbers of unfolding features and molecules, respectively.

nm, Figures 3a and S7) is consistent with that expected for a fully folded hairpin (expected ΔL 14.3 nm, see SI for calculation). Inside the nanocage with a 15 \times 15 nm cross section, the hairpins were also fully folded as revealed by the ΔL histograms (Figures 3a and S7, $\Delta L \approx 13.2$ nm). Therefore, the much-reduced unfolding/refolding force of the hairpin within the nanocage with respect to that outside (Figures 3b

and S6) must be due to the different environment inside the nanocage. This result demonstrated that hairpin duplex DNA in nanoconfinement has a surprisingly large reduction in the mechanical stability. The unexpected large reduction was also observed in the thermodynamic stability of the hairpin when the change in free energy of hairpin unfolding ($\Delta G_{\rm unfold}$) was estimated from the unfolding work using the Jarzynski equality expression²⁴ (25.1:6.4 kcal/mol (outside:inside nanocage), see Figures 3c and S12 for unfolding work histograms). It is noteworthy that $\Delta G_{\rm unfold}$ calculated by the Jarzynski equality is identical to that calculated by the mfold method²⁵ (Figure S13).

Unfolding Free Energy Profiles of the bcl-2 DNA Hairpin. Next, we retrieved the free energy profile of the entire unfolding trajectory of the bcl-2 hairpin using reported methods. 26,27 To this end, we collected hundreds of unfolding/ refolding events of the DNA hairpins within and without the nanocage. To account for baseline drifts due to different molecules, we calculated the change in contour length (ΔL) between the stretching and the relaxing force—extension curves (Figure 4a and 4b, left) during the force range in which folding and unfolding transitions occur.²⁸ Three force regions are shown in the $\Delta L - F$ plots (Figure 4a and 4b, middle). Right at the transition force, the positive and negative ΔL populations reflect the unfolding and refolding transitions, respectively, between the folded and the unfolded hairpins. At a force smaller than the hairpin transition, ΔL reduces to zero, which indicates folded hairpins in both stretching and relaxing F-Xcurves. At a force larger than the hairpin transition, ΔL reduces to zero again, corresponding to the unfolded hairpin in both stretching and relaxing F-X curves. Change in free energy

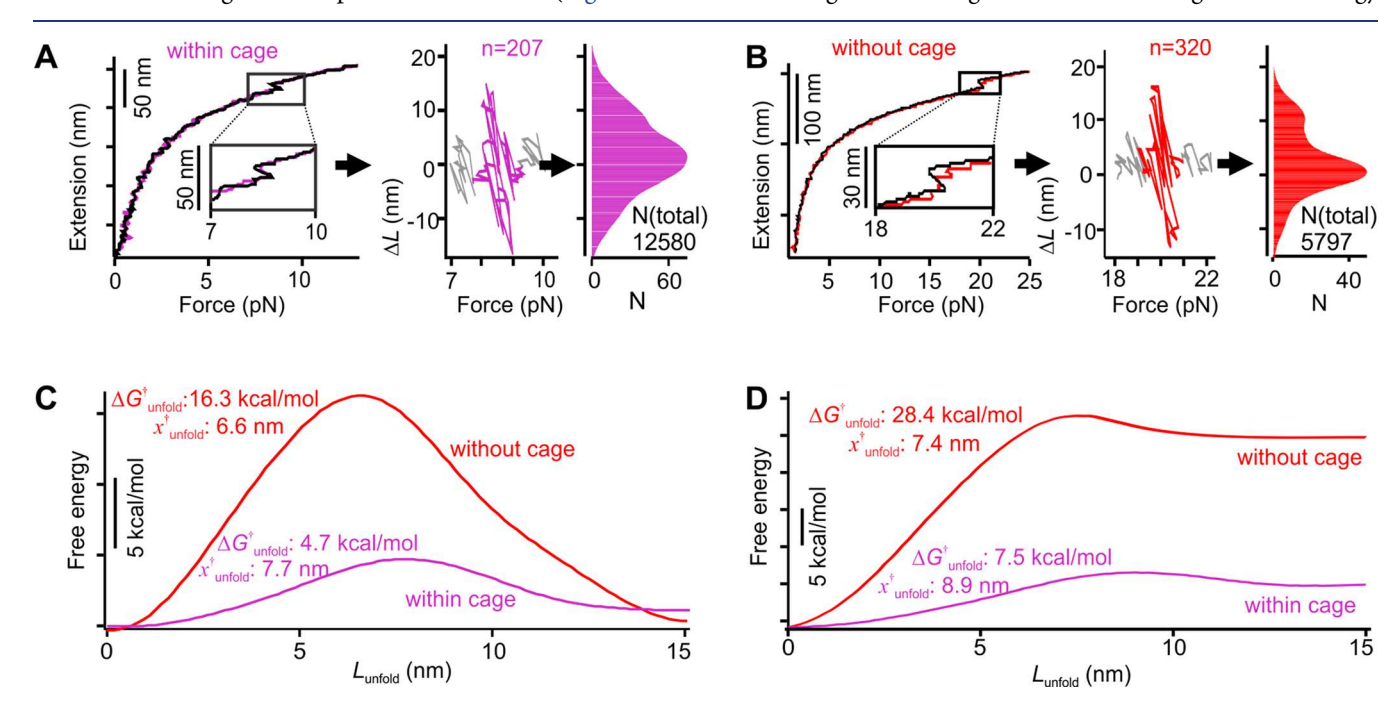


Figure 4. Unfolding free energy profiles of the bcl-2 hairpin. Population density profiles of the bcl-2 hairpin at the transition forces within (A) and without (B) the 15×15 nm nanocage. (Left) Extension vs force traces of the hairpin. Colored and black traces depict stretching and relaxing processes, respectively. Change in contour length (ΔL) versus force (F) plots (middle) are calculated based on the difference in the extension between the stretching and the relaxing traces at the same force around the transition events. Colors in the middle panels depict the unfolding and refolding transitions of the hairpin. Right panels show population profiles of the corresponding ΔL -F plots in the middle panels. Only populations with positive ΔL are used to obtain the unfolding energy profiles of the hairpin. n depicts the number of transition events used for analyses. Unfolding energy profile of the bcl-2 hairpin without (red) and within (purple) the nanocage at specific unfolding forces (C) and zero force (D). See text for notations.

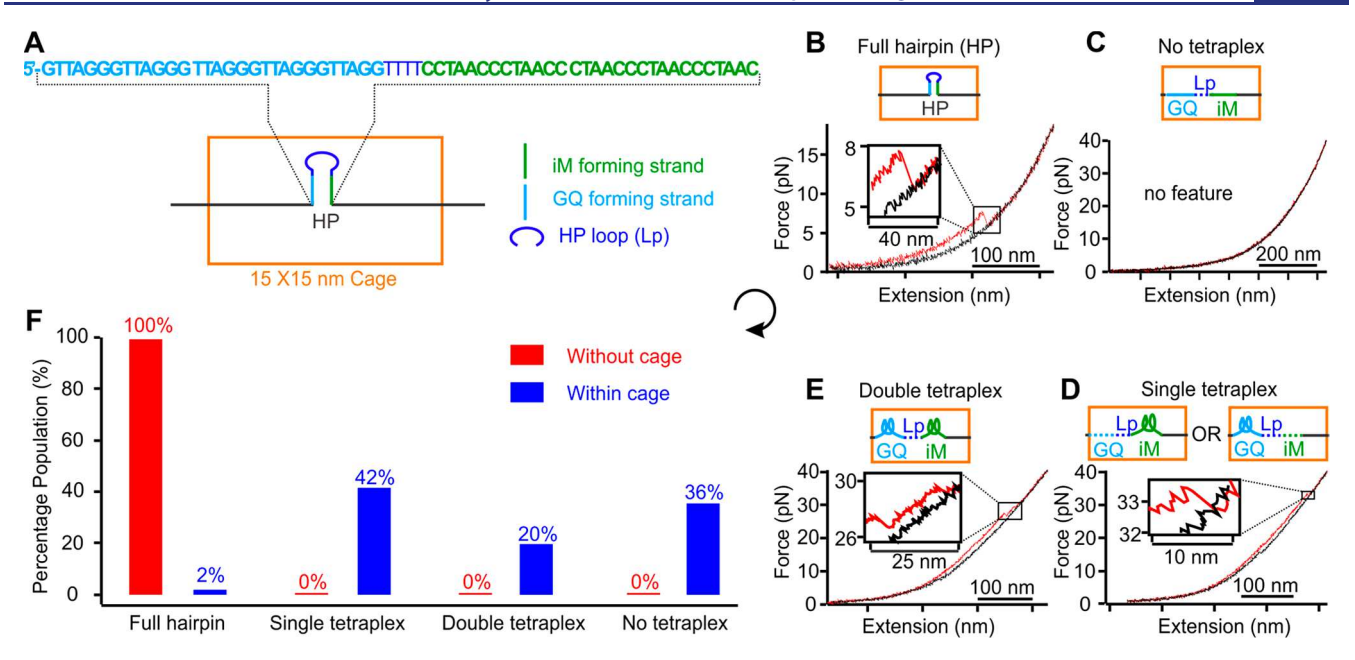


Figure 5. Competitive formation of B-DNA versus non-B DNA in nanoconfinement. (A) Schematic of a 15×15 nm nanocage that contains a hairpin with i-motif (iM) and G-quadruplex (GQ) forming sequences in complementary strands in the hairpin stem. Typical force versus extension curves of the hairpin inside nanoconfinement showing (B) full hairpin, (C) no tetraplex, (D) single tetraplex, and (E) double tetraplex formations. (F) Percentage populations of folded species without (red) and within (blue) the nanocage. Assignment of folded structures in each hairpin is based on ΔL and unfolding force histograms (see text and Figure S8; see Figure S9 for all observed structures). Note the "No tetraplex" population contains 8% partially folded hairpins. These experiments were performed in a 10 mM MES buffer (pH 5.5) supplemented with 100 mM KCl, 10 mM MgCl₂, and 1 mM EDTA at 25 °C.

 $(\Delta G(L, F))$ along the unfolding coordinate $(L_{\rm unfold})$ at a particular force (F) can be calculated by the Boltzmann equation, $\Delta G(L,F) = k_{\rm B}T \ln[P(L)]$, where P(L) is the population probability density. By grouping all unfolding transitions of the hairpins around the transition force (Figure 4a and 4b, right, only positive ΔL was considered), we were able to deconvolute the probability density P and obtain the unfolding free energy trajectory of the bcl-2 hairpin (Figure 4c) using a point spread function (PSF), which was obtained from the same DNA handles without hairpin forming sequence at a specific transition force (Figure S14).

To retrieve the unfolding free energy profile at F = 0 pN (Figure 4d), we further accounted for the energies stored in the dsDNA, in the unfolded hairpin, as well as in the two optical traps²⁶ (see SI). As these energies are either constant, which does not influence the shape of the free energy profile, or linearly proportional with respect to the reaction coordinate L_{unfold} , they contribute linearly to the final free energy profile. Therefore, this linear energy correction was determined by the change in the free energy between fully folded and fully unfolded hairpin, ΔG_{unfold} (obtained by the Jarzynski equality, see above and SI). As shown in Figure 4d, we found that the energy barrier to unfold the DNA hairpin $(\Delta G_{\text{unfold}}^{\dagger})$ is much reduced inside the nanocage compared to that without. This observation is in contrast to the unfolding of the G-quadruplex and i-motif, which demonstrated much larger $\Delta G^{\dagger}_{unfold}$ in nanoconfinement.^{8,9} Significantly, we also found that the transition state of the hairpin in nanoconfinement at zero force is located closer to the unfolded state (the distance between the folded and the transition states, x^{\dagger}_{unfold} , is 8.9 nm, Figure 4d) than that observed in the free solution ($x^{\dagger}_{unfold} = 7.4 \text{ nm}$), indicating that the hairpin structure becomes softer in confined space.²⁹ This trend falls into the Leffler-Hammond postulate

that defines the correlation between the force and the position of the transition state. 30,31

Competitive Formation of the B-DNA versus non-B **DNA** in Nanoconfinement. Compared to the much increased stability of the DNA G-quadruplex and i-motif structures in DNA nanocages, 8,9 the drastically decreased stability in duplex DNA suggests that in the confinement of many cellular machineries, formation of non-B DNA structures, such as G-quadruplex and i-motif tetraplexes which employ Hoogsteen base pairs, can be preferred over duplex DNA. To test this hypothesis, we compared the formation probability of the hairpin duplex DNA and the tetraplex structures using a hairpin in which G-quadruplex and i-motif forming sequences are placed in the two complementary stem strands (Figure 5a). In this design, formation of the fully folded hairpin and either of the two tetraplexes (Gquadruplex or i-motif) are mutually exclusive. It is noteworthy that the nanocage with a 15×15 nm cross section can readily accommodate the hairpin presented in any orientation (the 30bp stem of the hairpin has 10.2 nm in length) (Figure S15e). After the DNA construct was placed inside the 15×15 nm nanocage (Figure S5), mechanical unfolding experiments were performed in a 10 mM MES buffer (pH 5.5) supplemented with 100 mM KCl, 10 mM MgCl₂, and 1 mM EDTA at 25 °C (Figures 5b-e, S8, S9, and S11). Previous studies have demonstrated that the telomeric G-quadruplex and i-motif³² as well DNA hairpins³³ can form under similar conditions (pH 5.5 and 100 mM KCl).

Each of the two tetraplexes is expected to have a higher unfolding force and lower ΔL than fully folded hairpins (Figure S8). Therefore, from the magnitude of the ΔL and the rupture force associated with each unfolding feature in individual F-X traces, we were able to identify folded structures in the hairpin (Figures 5 and S9). We revealed

that only 2% population was fully folded hairpin, whereas 42% and 20% were single- and double-tetraplex structures, respectively, inside the 15×15 nm nanocage (Figures 5f and S9). In comparison, without the nanocage (Figure S8a and S8b), the population was exclusively a fully folded hairpin. These results confirmed that the B-DNA was weaker than the non-B DNA tetraplex structures in nanoconfinement.

DISCUSSION

At the molecular level, it has been shown that increased unfolding energy barriers for G-quadruplex and i-motif in nanoconfinement are due to the hydration of water molecules during the transition.9 In the nanocavity confined by charged walls such as those in the DNA origami nanoassembly, water molecules are well aligned with reduced activities due to increased ion-dipole interactions.8 Therefore, it is more difficult to interact with water in the nanocage during unfolding of the DNA tetraplexes, which increases the energy barrier. In duplex DNA, the much decreased stability of dsDNA was observed in molecularly crowded solution at a similar ionic strength, which is fully consistent with what we observed here.³⁴ The decreased stability was ascribed to the cosolute-mediated hydration during hybridization of duplex DNA.³⁴ Without cosolute, investigations now indicated the release of water molecules during the folding of duplex DNA.¹ However, it has been found that in the minor groove of duplex DNA, binding of the water molecule becomes much tighter compared to the ssDNA, whereas no significant difference is found for the phosphate group or the major groove. 15 The much compromised stability of duplex DNA in the nanocage can be attributed to this predominating enthalpic factor. Inside the DNA origami nanocage, water molecules with much reduced activities9 are sluggish to tightly interact with the minor groove of the dsDNA, which decreases the stability of the duplex DNA in the nanocage. In other studies, similar destabilization effect on the duplex DNA in solutions of reduced water activity has been attributed to the weakening of the base stacking in duplex DNA. 16,35 Molecular simulation revealed that the stem of the hairpin inside the nanocage is located toward the walls of the nanocage (Figure S15A, S15B, S15D, and S15E), which presented lower water activities compared to the center of the nanocage due to increased iondipole interactions close to the nanocage surface. After quantification of this geometrical effect, we found reduced water activity contributed at least 87% of reduced stability of the 17-bp bcl-2 hairpin inside the 15 × 15 nm nanocage (see SI, Figure S16). Other than the water activity effect, it is also possible that cations interacting with the negatively charged origami surface may result in reduced cation activity in nanoconfinement, which compromises the stability of duplex DNA by the reduced charge screening effect. In addition, the repulsive force between the DNA hairpin and the nanocage wall may destabilize the hairpin structure. This is because the unfolded form of the hairpin (ssDNA) is expected to maintain a longer distance to the nanocage wall due to its more flexible nature with respect to the duplex DNA in the hairpin stem. Molecular dynamics simulation can be used to better understand these different factors on the stability of DNA structures^{36,37} in nanoconfinement.

The surprisingly low stabilities of B-DNA in nanoconfinement give ramifications to correctly interpret results obtained from experiments where duplex DNA is imaged or analyzed in nanochannels or nanopores, especially with negatively charged

surfaces. This behavior is also of high physiological significance. Inside cells, DNA can be temporarily confined in many machineries employed for processes such as transcriptions and replications. Our results indicate that nanoconfinement weakens B-DNA, making it easier to unwind DNA duplex for biochemical processes such as formation of the open complex during transcription initiation or propagation of the transcription bubble.³⁸ At the same time, noncanonical DNA structures in the same DNA region become more stable in the confinement.^{8,9} As a result, population equilibrium shifts to favor the formation of non-B DNA structures. As these noncanonical structures have demonstrated regulatory roles,³⁹ the nanoconfinement can offer a unique way to modulate cellular processes. From this perspective, the nanoconfinement bears similarity to other cellular environments such as molecular crowding¹² and torsionally constrained DNA templates.^{40,41} Whereas the former condition often has a global effect applicable to the entire system at the steady state, the latter is quite dynamic in nature. 40 The nanoconfinement, however, provides a localized environment with its efficacy determined by the availability as well as the number of cellular machineries (or nanocavities) working on DNA templates.

CONCLUSIONS

By mechanical unfolding and refolding of DNA hairpins inside a DNA origami nanocage using optical tweezers, we quantified the property of B-DNA in nanoconfinement. We found both mechanical and thermodynamic stabilities of B-DNA hairpin decrease to unexpectedly low levels inside the nanocavity. Direct comparison for the formation of hairpin duplex DNA versus tetraplex DNA revealed preferential formation of tetraplex structures. These surprising results shed light on many in vivo or in vitro processes in which DNA and associated components are confined inside nanochannels, nanopores, or nanoreaction sites. They reveal a new pathway by which non-B DNA structures become preferred species in the context of double-stranded DNA, which justifies purported regulatory roles of noncanonical DNA structures for many biochemical processes inside cells.

ASSOCIATED CONTENT

Supporting Information

The Supporting Information is available free of charge at https://pubs.acs.org/doi/10.1021/jacs.0c01978.

Synthesis of the DNA origami nanocages that contain hairpin-hosting DNA fragment, synthesis strategy for the single-stranded DNA containing the bcl-2 hairpinforming sequence, synthesis strategy for the singlestranded DNA that contains a telomeric G-quadruplex sequence and a telomeric i-motif sequence, characterization of the single-molecular DNA nanocage constructs by AFM, unfolding/refolding force and change in contour length measurements, percentage populations of the hairpin and tetraplex structures, unfolding force versus extension plots, expected change-in-contourlength (ΔL) , calculation of the change in free energy of unfolding (ΔG_{unfold}), estimation of change in free energy of hairpin unfolding using mfold, energy stored in the unfolding pathway of the bcl-2 hairpin, point spread function used to convert species populations to relative free energies, coarse-grained molecular dynamics (MD)

simulation of the bcl-2 hairpin inside the nanocages, quantitation of factors in the reduced stability of the duplex DNA, supplemental references (PDF)

AUTHOR INFORMATION

Corresponding Authors

Hiroshi Sugiyama — Department of Chemistry, Graduate School of Science and Institute for Integrated Cell—Material Sciences, Kyoto University, Sakyo, Kyoto 606-8502, Japan; ⊙ orcid.org/0000-0001-8923-5946; Email: hs@kuchem.kyoto-u.ac.jp

Masayuki Endo — Department of Chemistry, Graduate School of Science and Institute for Integrated Cell—Material Sciences, Kyoto University, Sakyo, Kyoto 606-8502, Japan; ⊚ orcid.org/0000-0003-0957-3764; Email: endo@kuchem.kyoto-u.ac.jp

Hanbin Mao — Department of Chemistry & Biochemistry, Kent State University, Kent, Ohio 44242, United States; orcid.org/0000-0002-6720-9429; Email: hmao@kent.edu

Authors

Sagun Jonchhe — Department of Chemistry & Biochemistry, Kent State University, Kent, Ohio 44242, United States; orcid.org/0000-0003-4361-6641

Shankar Pandey — Department of Chemistry & Biochemistry, Kent State University, Kent, Ohio 44242, United States;
orcid.org/0000-0001-5576-6714

Deepak Karna — Department of Chemistry & Biochemistry, Kent State University, Kent, Ohio 44242, United States; orcid.org/0000-0003-3370-0997

Pravin Pokhrel — Department of Chemistry & Biochemistry, Kent State University, Kent, Ohio 44242, United States

Yunxi Cui — Department of Chemistry & Biochemistry, Kent State University, Kent, Ohio 44242, United States;

orcid.org/0000-0002-3830-3336

Shubham Mishra — Department of Chemistry, Graduate School of Science and Institute for Integrated Cell—Material Sciences, Kyoto University, Sakyo, Kyoto 606-8502, Japan

Complete contact information is available at: https://pubs.acs.org/10.1021/jacs.0c01978

Notes

The authors declare no competing financial interest.

ACKNOWLEDGMENTS

H.M. is thankful for financial support from the National Science Foundation [CHE-1904921] and National Institutes of Health [NIH 1R01CA236350]. This work was supported by a Grant-in-Aid for Scientific Research JSPS KAKENHI Fund for the Promotion of Joint International Research (Fostering Joint International Research (B)) (Grant Numbers 18KK0139 and 16H06356) to H.S. and M.E. Financial support from the Nakatani Foundation and the Uehara Memorial Foundation to M.E. is acknowledged. We thank Tomoko Emura and Kumi Hidaka for preparation of the DNA hairpin inside the nanocage.

REFERENCES

- (1) Persson, F.; Tegenfeldt, J. O. DNA in nanochannels—directly visualizing genomic information. *Chem. Soc. Rev.* **2010**, *39* (3), 985–999.
- (2) Clarke, J.; Wu, H.-C.; Jayasinghe, L.; Patel, A.; Reid, S.; Bayley, H. Continuous base identification for single-molecule nanopore DNA sequencing. *Nat. Nanotechnol.* **2009**, *4* (4), 265–270.

- (3) Jin, Q.; Fleming, A. M.; Burrows, C. J.; White, H. S. Unzipping Kinetics of Duplex DNA Containing Oxidized Lesions in an α -Hemolysin Nanopore. *J. Am. Chem. Soc.* **2012**, 134 (26), 11006–11011
- (4) Mitchell, M.; Gillis, A.; Futahashi, M.; Fujiwara, H.; Skordalakes, E. Structural basis for telomerase catalytic subunit TERT binding to RNA template and telomeric DNA. *Nat. Struct. Mol. Biol.* **2010**, *17* (4), 513–518.
- (5) Zhou, H.-X.; Dill, K. A. Stabilization of Proteins in Confined Spaces. *Biochemistry* **2001**, *40* (38), 11289–11293.
- (6) Takagi, F.; Koga, N.; Takada, S. How protein thermodynamics and folding mechanisms are altered by the chaperonin cage: Molecular simulations. *Proc. Natl. Acad. Sci. U. S. A.* **2003**, *100* (20), 11367–11372.
- (7) Brinker, A.; Pfeifer, G.; Kerner, M. J.; Naylor, D. J.; Hartl, F. U.; Hayer-Hartl, M. Dual Function of Protein Confinement in Chaperonin-Assisted Protein Folding. *Cell* **2001**, *107* (2), 223–233.
- (8) Shrestha, P.; Jonchhe, S.; Emura, T.; Hidaka, K.; Endo, M.; Sugiyama, H.; Mao, H. Confined space facilitates G-quadruplex formation. *Nat. Nanotechnol.* **2017**, *12* (6), 582–588.
- (9) Jonchhe, S.; Pandey, S.; Emura, T.; Hidaka, K.; Hossain, M. A.; Shrestha, P.; Sugiyama, H.; Endo, M.; Mao, H. Decreased water activity in nanoconfinement contributes to the folding of G-quadruplex and i-motif structures. *Proc. Natl. Acad. Sci. U. S. A.* **2018**, *115* (38), 9539–9544.
- (10) Pramanik, S.; Nagatoishi, S.; Sugimoto, N. DNA tetraplex structure formation from human telomeric repeat motif (TTAGGG): (CCCTAA) in nanocavity water pools of reverse micelles. *Chem. Commun.* **2012**, *48* (40), 4815–4817.
- (11) Zhou, J.; Wei, C.; Jia, G.; Wang, X.; Feng, Z.; Li, C. Formation and stabilization of G-quadruplex in nanosized water pools. *Chem. Commun.* **2010**, *46* (10), 1700–1702.
- (12) Miyoshi, D.; Karimata, H.; Sugimoto, N. Hydration Regulates Thermodynamics of G-Quadruplex Formation under Molecular Crowding Conditions. *J. Am. Chem. Soc.* **2006**, *128* (24), 7957–7963.
- (13) Zhao, C.; Ren, J.; Qu, X. Single-Walled Carbon Nanotubes Binding to Human Telomeric i-Motif DNA Under Molecular-Crowding Conditions: More Water Molecules Released. *Chem. Eur. J.* **2008**, *14*, 5435–5439.
- (14) Son, I.; Shek, Y. L.; Dubins, D. N.; Chalikian, T. V. Hydration Changes Accompanying Helix-to-Coil DNA Transitions. *J. Am. Chem. Soc.* **2014**, *136* (10), 4040–4047.
- (15) Nakano, M.; Tateishi-Karimata, H.; Tanaka, S.; Tama, F.; Miyashita, O.; Nakano, S.-i.; Sugimoto, N. Local thermodynamics of the water molecules around single- and double-stranded DNA studied by grid inhomogeneous solvation theory. *Chem. Phys. Lett.* **2016**, *660*, 250–255.
- (16) Feng, B.; Sosa, R. P.; Mårtensson, A. K. F.; Jiang, K.; Tong, A.; Dorfman, K. D.; Takahashi, M.; Lincoln, P.; Bustamante, C. J.; Westerlund, F.; Nordén, B. Hydrophobic catalysis and a potential biological role of DNA unstacking induced by environment effects. *Proc. Natl. Acad. Sci. U. S. A.* **2019**, *116* (35), 17169–17174.
- (17) Khimji, I.; Shin, J.; Liu, J. DNA duplex stabilization in crowded polyanion solutions. *Chem. Commun.* **2013**, 49 (13), 1306–1308.
- (18) Moriyama, R.; Iwasaki, Y.; Miyoshi, D. Stabilization of DNA Structures with Poly(ethylene sodium phosphate). *J. Phys. Chem. B* **2015**, *119* (36), 11969–11977.
- (19) Zinchenko, A.; Tsumoto, K.; Murata, S.; Yoshikawa, K. Crowding by Anionic Nanoparticles Causes DNA Double-Strand Instability and Compaction. *J. Phys. Chem. B* **2014**, *118* (5), 1256–1262.
- (20) Woodside, M. T.; Behnke-Parks, W. M.; Larizadeh, K.; Travers, K.; Herschlag, D.; Block, S. M. Nanomechanical measurements of the sequence-dependent folding landscapes of single nucleic acid hairpins. *Proc. Natl. Acad. Sci. U. S. A.* **2006**, 103 (16), 6190–6195.
- (21) Huppert, J. L.; Balasubramanian, S. Prevalence of quadruplexes in the human genome. *Nucleic Acids Res.* **2005**, 33 (9), 2908–2916.
- (22) Cui, Y.; Koirala, D.; Kang, H.; Dhakal, S.; Yangyuoru, P.; Hurley, L. H.; Mao, H. Molecular Population Dynamics of DNA

- Structures in a Bcl-2 Promoter Sequence is Regulated by Small-molecules and the Transcription Factor hnRNP LL. *Nucleic Acids Res.* **2014**, *42*, 5755–5764.
- (23) Yu, Z.; Schonhoft, J. D.; Dhakal, S.; Bajracharya, R.; Hegde, R.; Basu, S.; Mao, H. ILPR G-Quadruplexes Formed in Seconds Demonstrate High Mechanical Stabilities. *J. Am. Chem. Soc.* **2009**, 131 (5), 1876–1882.
- (24) Collin, D.; Ritort, F.; Jarzynski, C.; Smith, S. B.; Tinoco, I. J.; Bustamante, C. Verification of the Crooks fluctuation theorem and recovery of RNA folding free energies. *Nature* **2005**, 437, 231–234.
- (25) Zuker, M. Mfold web server for nucleic acid folding and hybridization prediction. *Nucleic Acids Res.* **2003**, *31*, 3406–3415.
- (26) Woodside, M. T.; Anthony, P. C.; Behnke-Parks, W. M.; Larizadeh, K.; Herschlag, D.; Block, S. M. Direct Measurement of the Full, Sequence-Dependent Folding Landscape of a Nucleic Acid. *Science* **2006**, *314*, 1001–1004.
- (27) Koirala, D.; Punnoose, J. A.; Shrestha, P.; Mao, H. Yoctoliter thermometry for single-molecule investigations: A generic bead-on-atip temperature-control module. *Angew. Chem., Int. Ed.* **2014**, 53 (13), 3470–3474.
- (28) Yu, Z.; Gaerig, V.; Cui, Y.; Kang, H.; Gokhale, V.; Zhao, Y.; Hurley, L. H.; Mao, H. Tertiary DNA Structure in the Single-Stranded hTERT Promoter Fragment Unfolds and Refolds by Parallel Pathways via Cooperative or Sequential Events. *J. Am. Chem. Soc.* **2012**, *134* (11), 5157–5164.
- (29) Alemany, A.; Ritort, F. Force-Dependent Folding and Unfolding Kinetics in DNA Hairpins Reveals Transition-State Displacements along a Single Pathway. *J. Phys. Chem. Lett.* **2017**, 8 (5), 895–900.
- (30) LEFFLER, J. E. Parameters for the Description of Transition States. *Science* **1953**, *117* (3039), 340–341.
- (31) Hammond, G. S. A Correlation of Reaction Rates. *J. Am. Chem. Soc.* **1955**, *77* (2), 334–338.
- (32) Cui, Y.; Kong, D.; Ghimire, C.; Xu, C.; Mao, H. Mutually Exclusive Formation of G-Quadruplex and i-Motif Is a General Phenomenon Governed by Steric Hindrance in Duplex DNA. *Biochemistry* **2016**, 55 (15), 2291–2299.
- (33) Shrestha, P.; Cui, Y.; Wei, J.; Jonchhe, S.; Mao, H. A New Concentration Jump Strategy Reveals the Lifetime of i-Motif at Physiological pH without Force. *Anal. Chem.* **2018**, *90* (3), 1718–1724.
- (34) Nakano, M.; Tateishi-Karimata, H.; Tanaka, S.; Tama, F.; Miyashita, O.; Nakano, S.-i.; Sugimoto, N. Thermodynamic properties of water molecules in the presence of cosolute depend on DNA structure: a study using grid inhomogeneous solvation theory. *Nucleic Acids Res.* **2015**, *43* (21), 10114–10125.
- (35) Hormeño, S.; Ibarra, B.; Valpuesta, J. M.; Carrascosa, J. L.; Ricardo Arias-Gonzalez, J. Mechanical stability of low-humidity single DNA molecules. *Biopolymers* **2012**, *97* (4), 199–208.
- (36) Galindo-Murillo, R.; Roe, D. R.; Cheatham, T. E. Convergence and reproducibility in molecular dynamics simulations of the DNA duplex d(GCACGAACGAACGAACGC). *Biochim. Biophys. Acta, Gen. Subj.* 2015, 1850 (5), 1041–1058.
- (37) Panczyk, T.; Wojton, P.; Wolski, P. Mechanism of unfolding and relative stabilities of G-quadruplex and I-motif noncanonical DNA structures analyzed in biased molecular dynamics simulations. *Biophys. Chem.* **2019**, 250, 106173.
- (38) Djordjevic, M.; Bundschuh, R. Formation of the open complex by bacterial RNA polymerase–a quantitative model. *Biophys. J.* **2008**, 94 (11), 4233–4248.
- (39) Siddiqui-Jain, A.; Grand, C. L.; Bearss, D. J.; Hurley, L. H. Direct Evidence for a G-quadruplex in a Promoter Region and Its Targeting with a Small Molecule to Repress c-MYC Transcription. *Proc. Natl. Acad. Sci. U. S. A.* **2002**, *99*, 11593–11598.
- (40) Kouzine, F.; Liu, J.; Sanford, S.; Chung, H. J.; Levens, D. The dynamic response of upstream DNA to transcription-generated torsional stress. *Nat. Struct. Mol. Biol.* **2004**, *11* (11), 1092–100.

(41) Selvam, S.; Koirala, D.; Yu, Z.; Mao, H. Quantification of Topological Coupling between DNA Superhelicity and G-quadruplex Formation. *J. Am. Chem. Soc.* **2014**, *136*, 13967–13970.